Catalysis Letters Vol. 106, Nos. 1–2, January 2006 (© 2006)
DOI: 10.1007/s10562-005-9185-4

Methane oxidation over *M*–8YSZ and *M*–CeO_2/8YSZ (*M* = Ni, Cu, Co, Ag) catalysts

Masaki Itome, and Alan E. Nelson*

Department of Chemical and Materials Engineering, University of Alberta, Edmonton, Alberta, T6G 2G6, Canada

Received 30 June 2005; accepted 15 September 2005

The oxidation of methane has been studied by sequential flow reaction experiments over M–8YSZ and M–CeO_2/8YSZ (M = Ni, Cu, Co, Ag) catalysts as a function of CH_4/O_2 from 773 to 1073 K. Over Ni–8YSZ and Ni–CeO_2/8YSZ, methane pyrolysis is dominant leading to surface carbon formation at temperatures of 873 K and above. While the addition of ceria to Ni–8YSZ to produce Ni–CeO_2/8YSZ does not significantly affect the reaction kinetics, the activity of Cu–CeO_2/8YSZ, Co–CeO_2/8YSZ, and Ag–CeO_2/8YSZ are higher than their M–8YSZ counterparts. The activity of Co–CeO_2/8YSZ at high temperatures (973 K and above) is higher than Ni-8YSZ with selectivity towards partial methane oxidation and CO formation. Considering Ni-based catalysts are prone to deactivation due to surface carbon accumulation, Co–CeO_2/8YSZ, Cu–CeO_2/8YSZ, and Ag–CeO_2/8YSZ are possible alternative anode cermets for direct hydrocarbon oxidation solid-oxide fuel cells (SOFC).

KEY WORDS: methane; oxidation; kinetics; carbon deposition; SOFC.

1. Introduction

The catalytic oxidation of methane is an important process for the production of clean energy from natural gas. In particular, the indirect utilization of methane as a fuel for solid-oxide fuel cells (SOFCs) has received recent attention due to advances in the synthesis and preparation of direct-oxidizing SOFC anode cermets [1,2]. The direct oxidation of methane in SOFCs offers significant advantages due to the higher open circuit voltage, as well as eliminating the need for internal or on-board reforming, leading to increased fuel utilization and efficiency. Current SOFCs utilize lanthanum strontium manganate (LSM) as the cathode, yttria-stabilized-zirconia (YSZ) at the electrolyte, and Ni–YSZ cermet as the anode [2]. These SOFCs are primarily limited to using hydrogen as the fuel, as opposed to methane, since the reaction of hydrocarbons on Ni–YSZ cermets results in carbon deposition and catalyst deactivation.

The oxidation of dry CH_4 over Ni-based catalysts results in the formation of carbon fibers above 973 K [3], and these fibres present a significant problem since they can completely occupy the anode surface in the SOFC. When used as a hydrocarbon reforming catalyst, carbon deposition can be mitigated by maintaining steam-to-hydrocarbon ratios greater than (typically) two [3,4]; however, this is not a practical solution for SOFC operation. Several studies have focused on alternative methane oxidation anode materials to overcome the issue of carbon deposition and deactivation, including attempts to modify Ni by incorporating other transition metals, such as manganese [5]. Steele *et al.* [6,7] have demonstrated direct conversion of methane using bismuth oxide, cerium dioxide, and $La_{0.8}Ca_{0.2}CrO_{3-x}$ anodes, and Putna *et al.* [8] found that direct oxidation of methane could be achieved using a Rh supported samaria-doped ceria anode. Ceria, an excellent electronic and ionic conductor, has also been shown to increase methane oxidation rates without coking [9]. Recently, Vohs and co-workers have demonstrated direct methane oxidation over M–CeO_2/YSZ (M = Ni, Cu) cermets [10,11], and have shown that Cu–CeO_2/YSZ cermets do not promote carbon deposition and are stable for extended periods operating on dry CH_4 [11]. The role of ceria, however, in enhancing methane oxidation over these M–CeO_2/YSZ (M = Ni, Cu) cermets is uncertain [12]. While ceria is used to enhance both ionic and electronic conductivity in the anode cermets and can also increase the active three-phase boundary in the anode, ceria is also an active catalyst for the oxidation of hydrocarbons [13]. However, Cu–CeO_2/YSZ cermets also demonstrated an overall decrease in efficiency, as evidenced by lower current densities compared to Ni–CeO_2/YSZ cermets [10,11].

Thus, the development highly active methane oxidation catalysts which mitigate carbon deposition at moderate operating temperatures have the clear potential to improve the usability of SOFCs. A replacement anode cermet to Ni–YSZ should be easy to process and maintain in the metallic state, and be catalytically inert with regards to carbon formation

* To whom correspondence should be addressed.
E-mail: alan.nelson@ualberta.ca

[12]. The catalyst must be economically practical since the anode must contain high concentrations of metal to maintain electrical conductivity. This precludes the use of precious metals, with the possible exception of silver [12]. In this work, we studied the oxidation of methane by sequential flow reaction experiments over M–8YSZ and M–CeO_2/8YSZ (M = Ni, Cu, Co, Ag) catalysts as a function of CH_4/O_2 from 773 to 1073 K. The results allow us to investigate the reaction kinetics and extent of carbon deposition, and suggest possible methane oxidation catalysts for further research as SOFC anode cermets.

2. Experimental

2.1. Catalyst preparation

The M–8YSZ (M = Ni, Cu, Co, Ag) catalysts were prepared by wet impregnation techniques using commercially available 8 mol% yttria-stabilized-zirconia (8YSZ, Tosoh, 14 $m^2\ g^{-1}$) and the following metal nitrate precursors: $Ni(NO_3)_2 \cdot 6H_2O$ (Aldrich, 99.9%); $Cu(NO_3)_2 \cdot 2.5H_2O$ (Aldrich, 99.9%); $Co(NO_3)_2 \cdot 6H_2O$ (Aldrich, 99.9%); and $AgNO_3$ (Aldrich, 99.9%). The catalysts were dried overnight at 373 K and subsequently calcined at 1223 K for 2 h in air. The ceria doped catalysts were prepared by physically mixing CeO_2 (Aldrich, 99.5%) with 8YSZ, and the M–CeO_2/8YSZ catalysts were prepared using the method previously described. The amounts of nitrate precursors were calculated and added to provide a final metal loading of 10 wt.%, and CeO_2 was incorporated to achieve a final loading of 20 wt.%.

2.2. Catalytic methane oxidation

The kinetics of methane oxidation were measured using 0.25 in. Pyrex tubular reactor operating at atmospheric pressure using approximately 400 mg of catalyst packed on a bed of quartz wool. The samples were initially reduced in 10% H_2/Ar (50 ml min^{-1}) using temperature-programmed reduction (TPR) with a heating rate of 10 K min^{-1}, followed by maintaining the catalysts at 1073 K for 20 min in the flowing hydrogen mixture. After reduction, a reactant mixture of methane and oxygen was introduced into the reactor with an inert (helium) to maintain a constant reactor flow rate. The reactant gas compositions included 25% CH_4/bal. He (Praxair) and 10% O_2/bal. He (Praxair), and the flow rates were adjusted using mass flow controllers to maintain a constant reactor inlet flow-rate of 60 ml min^{-1}. The methane to oxygen ratio was sequentially adjusted from $CH_4 : O_2 = 1 : 2$ (period A), $CH_4 : O_2 = 5 : 2$ (period B), $CH_4 : O_2 = 25 : 2$ (period C), $CH_4 : O_2 = 5 : 2$ (period D), to $CH_4 : O_2 = 1 : 2$ (period E) at reaction intervals of 20 min. Typical flow-rates for each period are as follows: 2.5 ml min^{-1} CH_4, 5 ml min^{-1} O_2, and 52.5 ml min^{-1} He (period A, E); 7.5 ml min^{-1} CH_4, 3 ml min^{-1} O_2, and 49.5 ml min^{-1} He (period B, D); 12.5 ml min^{-1} CH_4, 1 ml min^{-1} O_2, and 46.5 ml min^{-1} He (period C). The inlet concentrations were systematically varied to determine the effect of reactant composition on reaction rates, and provide an indication of catalyst deactivation due to carbon formation as a result of methane-rich oxidation. The reaction products were measured using a mass spectrometer, and subsequently quantified by measuring the intensity of the principal mass-to-charge (m/z) ratios. The conversion of methane was calculated based on the mass spectrum at the respective inlet compositions collected in the absence of a catalyst. Under the reaction conditions used in this study, the only significant reaction products detected were CO, CO_2, and H_2O.

3. Results and discussion

The steady-state values of methane and oxygen partial pressures were determined and subsequently used to describe the kinetics of methane oxidation over the catalysts studied. The experimental data were analyzed using differential flow reactor analysis assuming the reaction occurred rapidly in a shallow catalyst bed and the kinetics were not zero-order. For each experiment, the average rate of methane reaction was found using the following expression:

$$\frac{W_{\text{cat}}}{F_{\text{CH}_4,\text{out}}} = \int_{X_{\text{CH}_4,\text{in}}}^{X_{\text{CH}_4,\text{out}}} \frac{dX_{\text{CH}_4}}{-r_{\text{CH}_4}} = \frac{1}{(-r_{\text{CH}_4})_{\text{ave}}} \int_{X_{\text{CH}_4,\text{in}}}^{X_{\text{CH}_4,\text{out}}} dX_{\text{CH}_4} = \frac{X_{\text{CH}_4,\text{out}} - X_{\text{CH}_4,\text{in}}}{(-r_{\text{CH}_4})_{\text{ave}}} \quad (1)$$

where W_{cat} is the catalyst weight (g), F_{CH4} ,o is the initial methane flow-rate (mol min^{-1}), X_{CH4} is the conversion of methane, and $-r_{\text{CH4}}$ is the rate of methane reaction (molecules s^{-1} g_{cat}^{-1}). The conversion of methane was calculated assuming the carbon-containing reaction products from methane oxidation are CO and CO_2. While carbon accumulation was observed on the Ni-based catalysts, carbon deposition was not observed on the other catalysts. Each experimental run was analyzed to determine the average reaction rate at the average methane concentration in the differential flow reactor.

The rate of methane conversion for M–8YSZ and M–CeO_2/8YSZ catalysts for period A–C as a function of average methane partial pressure are shown in figures 1 and 2, respectively. Comparing the M–8YSZ catalysts (figure 1), Ni–8YSZ has the highest activity and the rate of reaction is nearly constant at temperatures of 873 K and above with a sharp decrease at 773 K. Co–8YSZ also demonstrated high reaction rates at temperatures of 973 K and above, however, the overall activity was significantly lower than Ni–8YSZ.

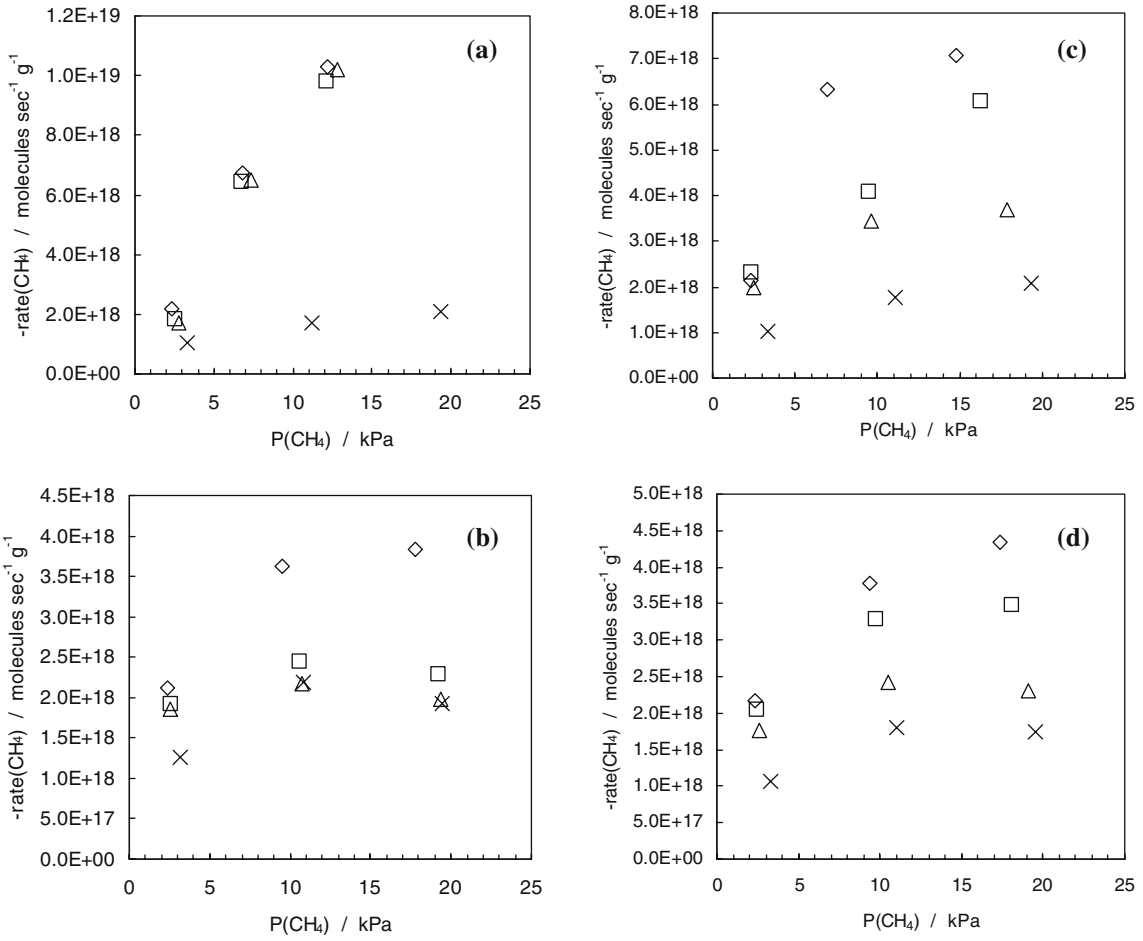

Figure 1. Rate of methane conversion for M–8YSZ for period A–C as a function of average methane partial pressure for (a) nickel, (b) copper, (c) cobalt, and (d) silver catalysts. The symbols correspond to the following temperatures: (◇) 1073 K; (□) 973 K; (△) 873 K; (×) 773 K.

Cu–8YSZ and Ag–8YSZ had comparable reaction rates over the entire temperature range, with Ag–8YSZ having better performance at 973 K. The addition of ceria to the catalysts produced variable results (figure 2). Examining the Ni-based catalysts, ceria incorporation slightly increased the reaction rates at temperatures of 973 K and above, with the rate at 873 K significantly lower for Ni–CeO_2/8YSZ than Ni–8YSZ and the rate at 773 K relatively unchanged. The kinetics over cobalt, copper, and silver based catalysts at intermediate temperatures are considerably improved following the addition of ceria. A significant increase in the reaction rates over Co–CeO_2/8YSZ at temperatures of 973 K and above were observed, with the rates at 973 K over Cu–CeO_2/8YSZ and Ag–CeO_2/8YSZ approaching the kinetics at 1073 K. This indicates ceria addition in copper, cobalt, and silver containing catalysts enhances the activity at intermediate temperatures (973 K), while no observable increase in activity was observed for nickel-based catalysts. The data also suggests Co–CeO_2/8YSZ catalysts at temperatures above 973 K have similar activity to Ni–8YSZ (and Ni–CeO_2/8YSZ), and the activity of Cu–CeO_2/8YSZ and Ag–CeO_2/8YSZ are enhanced through the addition of ceria.

The series or rate-concentration data was analyzed with a phenomenological rate expression to characterize the reaction order and estimate the activation energy associated with each catalyst composition. The results were expressed by the empirical rate expression:

$$(-r_{CH_4})_{ave} = kP^{\alpha}_{CH_4}P^{\beta}_{O_2} \qquad (2)$$

where k is the rate constant, P_{CH4} is the average partial pressure of methane, P_{O2} is the average partial pressure of oxygen, and α and β are the apparent reaction orders for methane and oxygen, respectively. Phenomenological rate expressions similar to equation (2) have been used previously by other researchers [14–16]. The apparent reaction orders and activation energy were determined by fitting the data to equation (2) modeling the temperature dependence on the rate expression using an Arrhenius relationship.

The calculated values of the apparent reaction orders and activation energy for each catalyst are summarized in tables 1 and 2. During the initial concentration periods (A–C), the M–8YSZ catalysts showed overall first order kinetics (approximately), with values of α ranging from 0.39 to 0.66 and values of β between −0.33 and

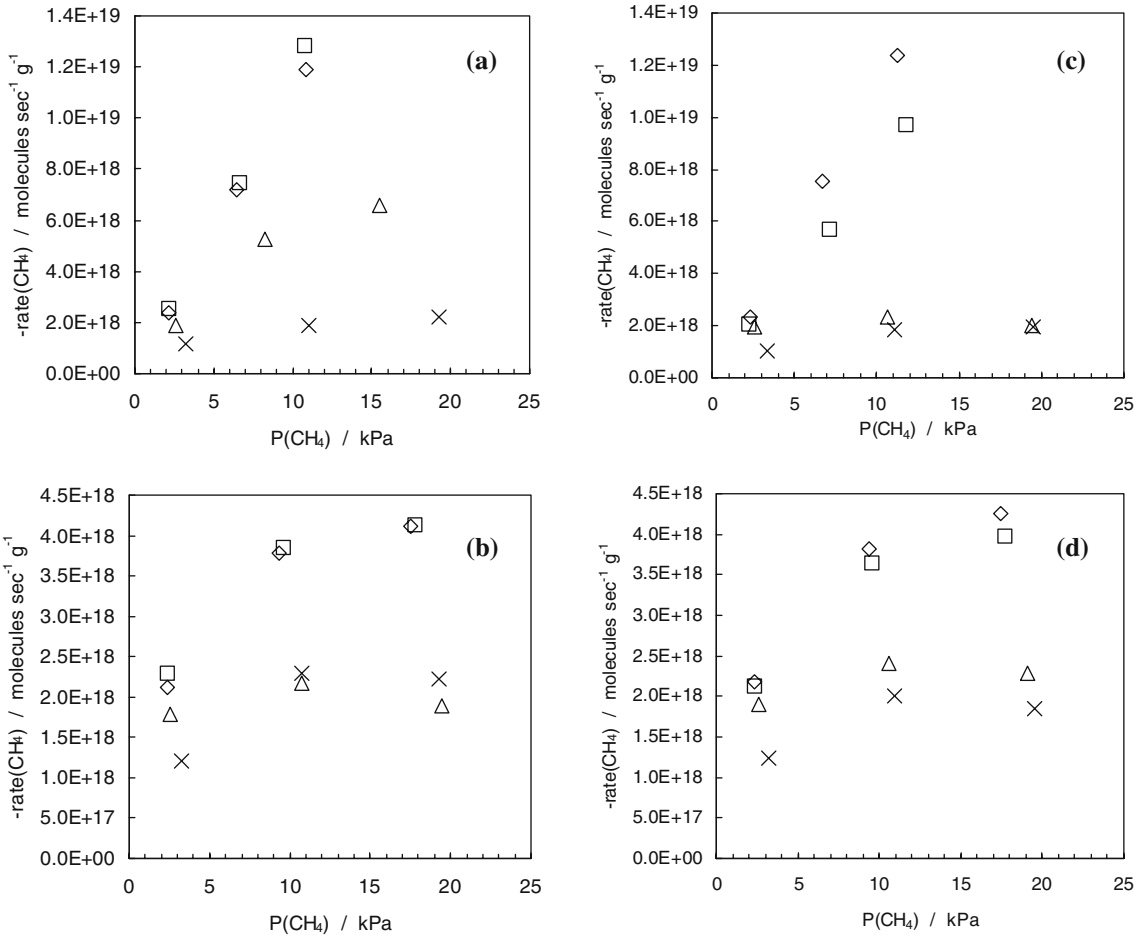

Figure 2. Rate of methane conversion for M–CeO_2/8YSZ for period A–C as a function of average methane partial pressure for (a) nickel, (b) copper, (c) cobalt, and (d) silver catalysts. The symbols correspond to the following temperatures: (◇) 1073 K; (□) 973 K; (△) 873 K; (×) 773 K.

0.32. The exception to this observation is Ni–8YSZ, which had a negative order of reaction with respect to oxygen ($\beta = -0.33$). The overall order of reaction for M–CeO_2/8YSZ catalysts was variable with values of α between 0.46 and 1.43 and values of β between 0.31 and 1.32, indicating inconsistent effects of CeO_2 addition, as noted previously. The apparent activation energies for M–8YSZ catalysts (Period A–C) varied from 15 kJ mol^{-1} (Cu—8YSZ) to 32 kJ mol^{-1} (Co–8YSZ), and ranged from 17 kJ mol^{-1} (Cu–CeO_2/8YSZ) to 47 kJ mol^{-1} (Co–CeO_2/8YSZ) for M–CeO_2/8YSZ catalysts. Ceria addition had little effect on the apparent activation energy for copper and silver based catalysts, while Ni–CeO_2/8YSZ and Co–CeO_2/8YSZ exhibited higher apparent activation energies in comparison with their M–8YSZ counterparts. For the second range of

Table 1
Phenomenological reaction orders, activation energies, and differential rates for methane oxidation for period A–C

	$(-r_{CH_4})_{ave} = kP^{\alpha}_{CH_4}P^{\beta}_{O_2}$			Differential rate[a]	
	α	β	Ea (±3 kJ mol^{-1})	1073 K (molecules s^{-1} g^{-1})	773 K (molecules s^{-1} g^{-1})
Ni–8YSZ	0.63	−0.33	30	2.2×10^{18}	1.0×10^{18}
Cu–8YSZ	0.39	0.32	15	2.1×10^{18}	1.3×10^{18}
Co–8YSZ	0.66	0.25	32	2.1×10^{18}	1.0×10^{18}
Ag–8YSZ	0.44	0.27	20	2.2×10^{18}	1.1×10^{18}
Ni–CeO_2/8YSZ	1.10	0.54	32	2.4×10^{18}	1.1×10^{18}
Cu–CeO_2/8YSZ	0.46	0.32	17	2.1×10^{18}	1.2×10^{18}
Co–CeO_2/8YSZ	1.43	1.32	47	2.4×10^{18}	1.0×10^{18}
Ag–CeO_2/8YSZ	0.46	0.31	18	2.2×10^{18}	1.2×10^{18}

[a]Differential rate of reaction for stoichiometric feed (CH_4 : $O_2 = 1 : 2$, period A).

Table 2
Phenomenological reaction orders, activation energies, and differential rates for methane oxidation for period C–E

	$(-r_{CH_4})_{ave} = kP^{\alpha}_{CH_4}P^{\beta}_{O_2}$			Differential rate[a]	
	α	β	Ea (±3 kJ mol^{-1})	1073 K (molecules s^{-1} g^{-1})	773 K (molecules s^{-1} g^{-1})
Ni–8YSZ	0.54	−0.27	29	2.1×10^{18}	1.1×10^{18}
Cu–8YSZ	0.21	0.07	14	2.1×10^{18}	1.3×10^{18}
Co–8YSZ	0.84	0.62	36	2.3×10^{18}	1.1×10^{18}
Ag–8YSZ	0.36	0.14	20	2.2×10^{18}	1.1×10^{18}
Ni–CeO_2/8YSZ	0.97	0.44	30	2.4×10^{18}	1.1×10^{18}
Cu–CeO_2/8YSZ	0.33	0.15	16	2.1×10^{18}	1.3×10^{18}
Co–CeO_2/8YSZ	1.29	1.00	47	2.6×10^{18}	1.1×10^{18}
Ag–CeO_2/8YSZ	0.31	0.10	18	2.2×10^{18}	1.3×10^{18}

[a]Differential rate of reaction for stoichiometric feed ($CH_4 : O_2 = 1 : 2$, period E).

partial pressures (Period C–E, table 2), the overall order of reaction varied significantly, with α values from 0.21 to 0.84 and β values from −0.27 to 0.62 for M–8YSZ. The reaction orders over M–CeO_2/8YSZ catalysts had values of α between 0.31 and 1.29 and β between 0.10 and 1.00. Of particular interest is the order of reaction with respect to oxygen for Ni–8YSZ and Ni–CeO_2/8YSZ catalysts, which are similar despite the observable accumulation of carbon fibers on the catalyst surface after experiment. The apparent activation energies are also unchanged during the second reaction period (C–E), indicating the main reaction pathway was unaffected by carbon accumulation.

Carbon deposition during methane oxidation is generally assumed to proceed via methane pyrolysis followed by carbon oxidation;

$$CH_4 \rightarrow C + 2H_2 \quad \Delta G_{298} = 50.45\,\text{kJ mol}^{-1} \qquad (3)$$

$$2C + O_2 \rightarrow 2CO \quad \Delta G_{298} = -274.3\,\text{kJ mol}^{-1} \qquad (4)$$

or via direct partial methane oxidation followed by carbon monoxide disproportionation;

$$2CH_4 + O_2 \rightarrow 2CO + 4H_2 \quad \Delta G_{298} = -173.4\,\text{kJ mol}^{-1} \qquad (5)$$

$$2CO \rightarrow C + CO_2 \quad \Delta G_{298} = -120.1\,\text{kJ mol}^{-1} \qquad (6)$$

It has been previously shown that SOFCs utilizing Ni–YSZ anode cermets can operate with dry methane without significant carbon deposition (coking) up to 100 h of operation [9]. Murray *et al.* [9] reported carbon-free methane oxidation over Ni-based cermets at operating temperatures between 773 and 973 K. At temperatures above 973 K, carbon formation proceeded according to reaction (3) while reaction (6) was effectively suppressed. At temperatures below 773 K, carbon deposition occurred via reaction (6) unless the CO/CO_2 ratio was relatively low.

Thus, it is suggested the primary reaction over Ni–8YSZ and Ni–CeO_2/8YSZ is methane pyrolysis followed by carbon oxidation. This is consistent with the inverse dependency on oxygen partial pressure, and is further supported by the high selectivity to CO formation over Ni–8YSZ and Ni–CeO_2/8YSZ at long contact times (tables 3 and 4). The formation of CO_2 is likely the result of CO disproportionation (equation 6) increasing the amount of surface carbon, which is consistent with the observed carbon deposition on Ni–8YSZ and Ni–CeO_2/8YSZ at high temperatures. At a temperature of 773 K, carbon accumulation was not observed over Ni–8YSZ and Ni–CeO_2/8YSZ indicating the moderate CO_2 and CO partial pressure ratios effectively prevent carbon deposition, as noted previously. The only other catalyst that demonstrated a change in the CO_2/CO ratio at high temperatures (973 K and above) was

Table 3
CO_2/CO selectivity over M–8YSZ catalysts as a function of reaction temperature and $CH_4 : O_2$ ratios (period A–E)

	Period	P_{CO2}/P_{CO}			
		1073 K	973 K	873 K	773 K
Ni–8YSZ	A	0.49	1.97	0.69	0.19
	B	0.03	0.02	0.06	0.21
	C	0.03	0.02	0.03	0.13
	D	0.05	0.03	0.07	0.21
	E	0.05	0.05	0.14	0.19
Cu–8YSZ	A	0.74	1.87	1.62	0.69
	B	0.40	0.95	0.89	0.95
	C	0.15	0.30	0.27	0.30
	D	0.39	0.98	0.85	0.93
	E	0.70	2.33	1.62	0.72
Co–8YSZ	A	1.11	0.52	0.57	0.20
	B	0.01	0.30	0.37	0.34
	C	0.02	0.04	0.13	0.23
	D	0.02	0.24	0.37	0.38
	E	0.02	0.56	0.59	0.22
Ag–8YSZ	A	0.55	0.73	1.24	0.51
	B	0.27	0.39	0.72	0.72
	C	0.10	0.14	0.23	0.29
	D	0.30	0.42	0.80	0.63
	E	0.61	0.79	1.13	0.49

Table 4
CO_2/CO selectivity over M–CeO_2/8YSZ catalysts as a function of reaction temperature and CH_4:O_2 ratios (period A–E)

	Period	P_{CO2}/P_{CO}			
		1073 K	973 K	873 K	773 K
Ni–CeO_2/8YSZ	A	0.48	0.46	2.03	0.29
	B	0.03	0.03	1.14	0.40
	C	0.02	0.02	0.04	0.21
	D	0.04	0.04	0.08	0.38
	E	0.04	0.06	0.27	0.29
Cu–CeO_2/8YSZ	A	0.70	0.58	2.04	0.34
	B	0.35	0.34	1.11	0.69
	C	0.14	0.12	0.32	0.26
	D	0.39	0.33	0.87	0.74
	E	0.65	0.58	1.63	0.44
Co–CeO_2/8YSZ	A	0.57	0.60	2.24	0.34
	B	0.02	0.03	1.15	0.64
	C	0.03	0.03	0.34	0.30
	D	0.04	0.05	1.13	0.71
	E	0.05	0.06	2.19	0.39
Ag–CeO_2/8YSZ	A	0.69	0.67	1.64	0.66
	B	0.37	0.36	0.86	0.79
	C	0.14	0.12	0.26	0.29
	D	0.37	0.35	0.86	0.88
	E	0.68	0.67	1.68	0.85

Co–8YSZ and Co–CeO_2/8YSZ, with the effect more pronounced for the ceria-containing catalyst. Because significant carbon accumulation was not observed on the cobalt-containing catalysts, it is suggested the primary oxidation mechanism is the partial oxidation of methane. Carbon monoxide disproportionation cannot be excluded, but this could be accompanied by carbon oxidation to eliminate surface carbon. The irreversible selectivity towards CO_2 at high temperatures (973 K and above) over cobalt-based catalysts is further evidence to support these observations. The copper and silver containing catalysts showed reversible selectivity towards CO_2 at all temperatures, and no carbon accumulation was noted over these catalysts with relatively high methane conversion activity. Thus, it is likely methane conversion proceeds via balanced complete and partial methane oxidation.

It should also be noted that at lower temperatures (773–873 K), an increase in the CO_2/CO ratio was observed for all M–CeO_2/8YSZ catalysts. Ceria is a well-known oxygen storage material, and may be providing atomic oxygen to react with CO adsorbed at the metal–metal oxide interface to increase the CO_2/CO ratio at these temperatures. However, the precise role of ceria in enhancing the results for methane oxidation in this study is uncertain. As noted previously, ceria enhances both ionic and electronic conductivity in anode cermets which is suggested to increase the active three-phase boundary region [9]. Coupled with the enhanced oxygen storage and transport ability, an increase in the three-phase boundary would be expected to increase methane oxidation rates. The present study indicates this effect is more pronounced for Cu–CeO_2/8YSZ, Co–CeO_2/8YSZ and Ag–CeO_2/8YSZ catalysts compared to Ni–CeO_2/8YSZ.

4. Conclusions

Ni–8YSZ and Ni–CeO_2/8YSZ methane oxidation catalysts demonstrated high activity, but with selectivity towards surface carbon formation. The inverse dependency with regards to oxygen partial pressure and the accumulation of surface carbon suggests the primary reaction over the Ni-based catalysts is methane pyrolysis. The addition of ceria to Co–8YSZ increased the rate of methane conversion at high temperatures (973 K and above), however, the irreversible CO_2 selectivity indicates partial methane oxidation leading to CO formation would be the primary reaction at long reaction times. Ceria addition in copper, cobalt, and silver containing catalysts enhances the activity at intermediate temperatures (973 K), while no observable increase in activity was observed for nickel-based catalysts. Considering Ni-based catalysts are prone to deactivation due to surface carbon accumulation, Co–CeO_2/8YSZ, Cu–CeO_2/8YSZ, and Ag–CeO_2/8YSZ are possible alternative anode cermets for direct hydrocarbon oxidation SOFC. Additional research is required, however, to increase the activity of Co–CeO_2/8YSZ and Ag–CeO_2/8YSZ and assess the I–V relationships and power levels.

Acknowledgements

This work is supported by the Natural Sciences and Engineering Research Council (NSERC) Discovery Grant program and the Alberta Energy Research Institute (AERI) under the Core University Research in Sustainable Energy (COURSE) program.

References

[1] J. Liu and S.A. Barnett, Solid State Ionics 158 (2003) 11.
[2] S.C. Singhal and K. Kendall, *High Temperature Solid Oxide Fuel Cells; Fundamentals, Design, and Applications* (Elsevier, Oxford, 2003).
[3] C.H. Bartholomew, Catal. Rev.-Sci. Eng. 24 (1982) 67.
[4] J.N. Armor, Appl. Catal. A. 176 (1999) 159.
[5] S. Primdahl and M. Morgensen, in: SOCF VI, Proceedings of the 6th International Symposium (Electrochemical Society, Pennington, 1999, pp. 530).
[6] B.C.H. Steele, P.H. Middleton and R. Rudkin, Solid State Ionics 40/41 (1990) 388.
[7] R.T. Baker, I.S. Metcalfe, P.H. Middleton and B.C.H. Steele, Solid State Ionics 72 (1994) 328.
[8] E.S. Putna, J. Stubenraugh, J.M. Vohs and R.J. Gorte, Langmuir 11 (1995) 4832.
[9] E.P. Murray, T. Tsai and S.A. Barnett, Nature 400 (1999) 649.
[10] S. Park, J.M. Vohs and R.J. Gorte, Nature 404 (2000) 265.

[11] S. Park, R. Craciun, J.M. Vohs and R.J. Gorte, J. Electrochem. Soc. 146 (1999) 3603.
[12] R.J. Gorte, S. Park, J.M. Vohs and C. Wang, Adv. Mater. 12 (2000) 1465.
[13] A. Trovarelli, Catal. Rev.-Sci. Eng. 38 (1996) 439.
[14] V.C. Belessi, A.K. Ladavos, G.S. Armatas and P.J. Pomonis, Phys. Chem. Chem Phys. 3 (2001) 3856.
[15] H. Arai, T. Yamada, E. Eguchi and T. Seiyama, Appl. Catal. 26 (1986) 265.
[16] M. Stojanovic, C.M. Mims, H. Moudallal, Y.L. Yang and A.J. Jacobson, J. Catal. 166 (1997) 324.